metals

MDPI

Article

Jet Penetration Performance of a Shaped Charge Liner Prepared by Metal Injection Molding

Zheyu He [1], Yi Cheng [2], Hao He [1,*], Chuanfeng An [3], Yuqing Huang [3], Xiang Zhang [3] and Yimin Li [1,3]

[1] School of Microelectronics and Materials Engineering, Guangxi University of Science and Technology, Liuzhou 545006, China; hezheyu@gxust.edu.cn (Z.H.); liyimin333@csu.edu.cn (Y.L.)
[2] School of Mechanical and Automotive Engineering, Guangxi University of Science and Technology, Liuzhou 545006, China; yiiiiiiiii99@gmail.com
[3] State Key Laboratory of Powder Metallurgy, Central South University, Changsha 410083, China; anchuanfeng1230@gmail.com (C.A.); jokerincs@163.com (Y.H.); xiangnpic@163.com (X.Z.)
* Correspondence: 100001865@gxust.edu.cn; Tel.: +86-139-7311-4617

Abstract: The metal injection molding (MIM) method was applied to manufacture a shaped charge liner (SCL) used for petroleum perforating bombs. Its application could overcome the drawback of heterogeneous density distribution prepared using the traditional powder metallurgy and spinning process. The sintering results showed that because of the limitation in the sintering temperature, the relative density of the W–Cu alloy shaped charge liners prepared by metal injection molding (MIM W–Cu SCLs) ranged from 48.05% at 1050 °C to 52.52% at 1100 °C, which was far below those prepared by spinning. Further increase to higher temperature led to the W–Cu separation, cracks, and distortion of the SCL. The explosive test proved that the shaped charge liners prepared by metal injection molding (MIM SCLs) could achieve comparable or even better penetration performance than those prepared by spinning. The particle size of tungsten played a significant role in the penetration performance in which the sample prepared from a −250-mesh tungsten powder showed the highest penetration depth, which was 18.44% deeper than that of the spinning process. From the observation of ballistic holes, the jet of the MIM SCL was composed of dispersed W–Cu particles without a slug. The diameters of the holes bored by the MIM SCLs were larger than those SCLs produced by spinning, which proved that the MIM SCL jet is noncoherent.

Keywords: shaped charge liner; W–Cu alloy; metal injection molding; jet

check for updates

Citation: He, Z.; Cheng, Y.; He, H.; An, C.; Huang, Y.; Zhang, X.; Li, Y. Jet Penetration Performance of a Shaped Charge Liner Prepared by Metal Injection Molding. *Metals* **2022**, *12*, 1021. https://doi.org/10.3390/met12061021

Academic Editor: Alberto Moreira Jorge Junior

Received: 26 April 2022
Accepted: 8 June 2022
Published: 16 June 2022

Publisher's Note: MDPI stays neutral with regard to jurisdictional claims in published maps and institutional affiliations.

Copyright: © 2022 by the authors. Licensee MDPI, Basel, Switzerland. This article is an open access article distributed under the terms and conditions of the Creative Commons Attribution (CC BY) license (https://creativecommons.org/licenses/by/4.0/).

1. Introduction

As a key part in petroleum perforation bullets, the properties of a shaped charge liner (SCL) play the most important role in determining the performance of a jet [1]. The traditional SCL manufacturing methods involve spinning, turning, stamping, forging, etc., which can produce SCLs with almost full density [2,3]. However, the extremely high hardness and inferior ductility of tungsten alloy make the SCLs difficult to machine, thereby increasing the cost of the production with a low efficiency [4]. Furthermore, the jet of these SCLs with a high relative density is always associated with serious slug phenomenon, which reduces the working mass of the SCL as well as the penetration performance [5]. Some researchers use the powder-metallurgy route such as cold press and sintering [6] to reduce the machining cost and improve the production rate. By adding elements with a low melting point, such as copper, nickel, iron, and so on, sintering of tungsten can be achieved within the conventional sintering temperature range, which can sustain the SCL preparation. Yan [7] reported that the tungsten SCL shows a good jet ductility because of the high density. However, the brittleness of tungsten at room temperature limits its application. Lu [8] studied the penetration performance of W-Ni-Fe alloy SCL, the results show that W-Ni-Fe alloy SCL can form ductility jet with a high velocity, but exhibit a low penetration. Bai [9] discovered that among pure W, W–Ni–Fe, and W–Cu SCLs prepared

using the P/M routes, the W–Cu SCL exhibits the best penetration performance. However, the conventional press and sintering method fails to produce an SCL with a uniform density distribution. Previous work reported that in pressed parts that were as large as the SCL, heterogeneous density distribution occurred not only in the pressing direction but also in the direction perpendicular to it, which could generate large pores, cracks, or distortions in the sintered parts [10]. As a result, the heterogeneous sintered density distribution leads to an unstable and asymmetric jet during explosion [11].

Metal injection molding (MIM) is a net-shaped method for producing complex-shaped parts with high performance, which can produce SCLs with high production rates and high level of automation [12]. Meanwhile, the forming process in MIM is achieved using the feedstock flow, which is composed of metal powder and organic binder. Thus, more uniform parts can be obtained [13]. More importantly, the flexible mold design of MIM allows easy production of SCLs with a specific shape such as a trumpet or double-V-cone shape, which can improve the penetration performance by increasing the explosive charge volume and jet speed [14]. Because of the difficulty in machining, research on complex-shaped SCLs is mainly confined in the simulation stage [15] although their large potential has been proven [16]. MIM is a feasible method for transforming this potential into reality. However, it is difficult achieving a relatively high-density MIM W–Cu alloy under most sintering conditions as a powder-metallurgy method. As a result, the penetration ability is uncertain because the jet may be discontinuous and noncoherent, which also reduces the penetration properties.

The current work manufactures W–20 Cu SCLs by MIM process. The density and microstructure of the sintered SCLs are investigated, and the penetration performance is tested. The effects of density, tungsten particle size, and mass of the SCLs on the penetration ability are studied. The characteristic of the explosive jets from MIM SCLs are also discussed. The results of this work can provide preliminary experimental data and optimization direction for MIM SCL production.

2. Experimental Procedures

The tungsten and copper powders were supplied by Hunan Injection High Technology Co., Ltd. (Changsha, China). The morphology is shown in Figure 1. To investigate the influence of the particle size, the tungsten powder has been sieved using −70, −180, −250, and −400-meshes, their particle size distribution is shown in Table 1. The tungsten and copper powders (mass ratio 4:1) were mixed using a paraffin wax-based binder (composed of paraffin wax, polypropylene, ethylene vinyl acetate and stearic acid) with total powder loading of 58% in an XSM1/20–80 rubber mixer at 130 °C for 120 min. The feedstock was injected into a V-type mold (OD = 31 mm, ID = 28 cm, and cone angle = 55°) on an HTF-90W2 injection molding machine (Haitian Machinery Co., Ltd., Ningbo, China). The injection temperature was 155 °C; the injection and holding pressure were 60 and 20 MPa respectively; the injection speed ranged from 50–60 mm/s; the injection and the holding time were 4 and 10 s respectively. The green parts are shown in Figure 2a. Some parts were broken after injection, which are mainly due to the difficulty in the injection of large samples. Short molding occurred because of the solidification of front feedstock or cold contraction. It is stressed that the yield rate exceeded 95%.

Table 1. Particle size distribution of tungsten powders.

Powder	D_{10}	D_{50}	D_{90}
Original	20.76 μm	83.21 μm	215.42 μm
−70-mesh	35.20 μm	100.53 μm	196.41 μm
−180-mesh	23.93 μm	47.66 μm	76.74 μm
−250-mesh	10.98 μm	25.69 μm	49.59 μm
−400-mesh	7.69 μm	21.47 μm	29.77 μm

A two-step debinding method consisting of solvent and thermal debinding was used to remove the binder. The green parts were solvent-debound at 40 °C for 120 min in methylene chloride, followed by thermal debinding and pre-sintering in argon gas at 900 °C for 60 min on a VSS-6611T debinding furnace (North Ture Vacuum Technology Co., Ltd., Shenyang, China). Then, the samples were sintered at different temperatures for 2 h under vacuum pressure of 10^{-1} Pa on a VHSgr40/150M vacuum sintering furnace (Shimadzu Co., Ltd., Tokyo, Japan). The as-sintered SCLs are shown in Figure 2b. A specific support frame was used in the sintering process to prevent distortion. The density of the sample was measured using the Archimedes method. The microstructures of the sintered samples were observed using a Polyvarmet metallurgical microscope (DM2700, Leica, Weztlar, Germany), and scanning electron microscopy (SEM) using a JSM-6360 microscope (JEOL, Tokyo, Japan) was performed to observe the steel plate and concrete target after the explosive test.

In the explosive test, the SH931 primary explosive with the mass of 1 g and R852 main explosive with the mass of 37 g were pressed with the SCL into a steel cylinder shell. Then, the shell was placed on top of two 45# steel plates with a height of 5 mm and a 1-m-high concrete target, as shown in Figure 3. After the explosion, the penetration depth of the concrete target was recorded, and at least three data were collected to obtain the average value for each condition. For comparison, spun W–20Cu SCLs with a 70 g mass were also tested. To investigate the effects of the sample mass, the preparation of some SCLs used contained a redesigned mold, and the height of the SCL mouth was increased to increase the total mass to 65 or 70 g. The amount of explosive powder and the standoff in all explosive tests were almost equivalent.

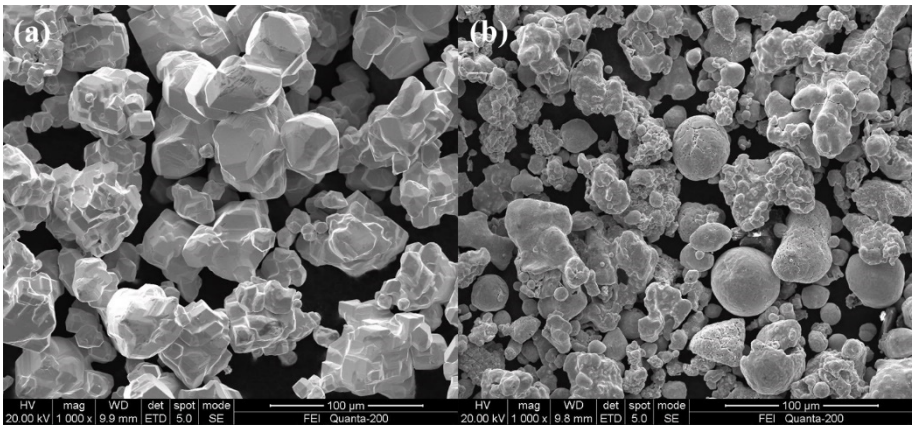


Figure 1. SEM images of. (**a**) Tungsten powder. (**b**) Copper powder.

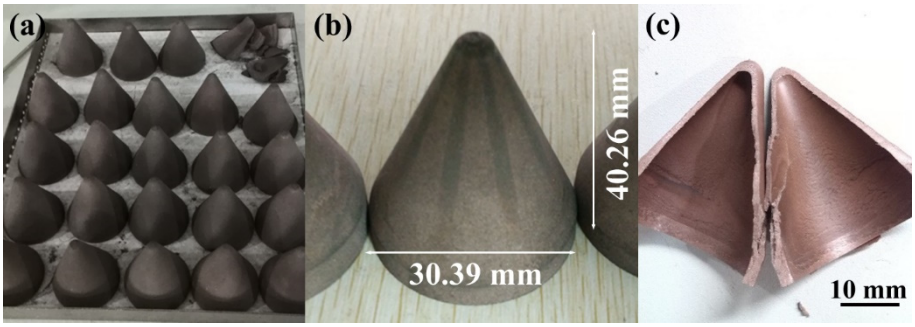


Figure 2. SCL prepared by the MIM process. (**a**) As-received green parts. (**b**) As-sintered parts. (**c**) As-sintered part with defects.

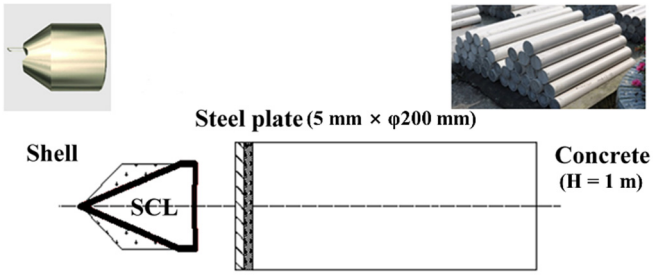


Figure 3. Schematic image of the explosive-test facilities.

3. Results and Discussion

3.1. Density and Microstructure

The density and microstructure of the MIM SCLs sintered from original powder under different temperatures are shown in Figure 4a. Density of samples sintered between 1050 and 1100 °C are listed in Table 2. All samples exhibit low density in the range of 48–56%. The melting point of the main component of tungsten is 3410 °C, which is much higher than the sintering temperature, resulting in a low densification rate. The sample sintered at 1050 °C exhibits a low density of 48.05%, which increases to 52.52% at elevated temperature of 1100 °C. Further increase to higher temperature does not lead to higher density. Instead, separation of the copper and tungsten phase can be observed, as shown in Figure 2c, where obvious cracks can be observed. Figure 4b shows that the copper powder (orange particles) retains its original near-spherical shape at 1050 °C, which indicates that sintering conducted in a solid stage and under a poor densification level is implemented. Higher temperature at 1100 °C leads to the melting of copper (melting point about 1083 °C). The existence of a liquid-copper phase promotes sintering, which then solidifies on the tungsten particles after sintering, as shown in Figure 4c. It is stressed that no W-Cu compound is found, which is in good accordance with the observation of Guo [2]. These two conditions indicate that the sample consists of discontinuous particles instead of a tungsten skeleton, and large number of interconnected pores are observed. After 1100 °C, increasing temperature leads to higher fluidity of the liquid copper. The melted copper flows to the inner surface of the sample; thus, a bronze surface is shown in Figure 2c. The separation of tungsten and copper phase exposed the discontinuous tungsten particles. The low-level conjunction of SCL leads to defects, distortion, and a decrease in density. In the sample sintered at 1500 °C, as shown in Figure 4d, the copper phase can rarely be observed, but a tungsten skeleton is formed. The density rapidly increases and reaches the highest value of approximately 56%. Although a higher sintering temperature (>1500 °C) can yield a high density, the separation of copper from the tungsten and the low yield rates are detrimental [17]. Thus, only the SCLs sintered at 1050 and 1100 °C are chosen for the subsequent experiments.

Table 2. Density and penetration performance of the MIM SCLs sintered under different conditions.

Powder	Sintering Temperature (°C)	Relative Density (%)	Penetration Depth (mm)	Size of Ballistic Hole (mm)
Original	1050	48.05	590	8.9 × 9.8
Original	1100	52.52	650	8.2 × 8.5
Spinning	-	78.44	591	5.6 × 6
−70-mesh	1100	52.6	565	7.9 × 8.2
−180-mesh	1100	52.4	615	8 × 8.5
−250-mesh	1100	52.7	700	8.4 × 8.9
−400-mesh	1100	52.7	520	8.7 × 9.3

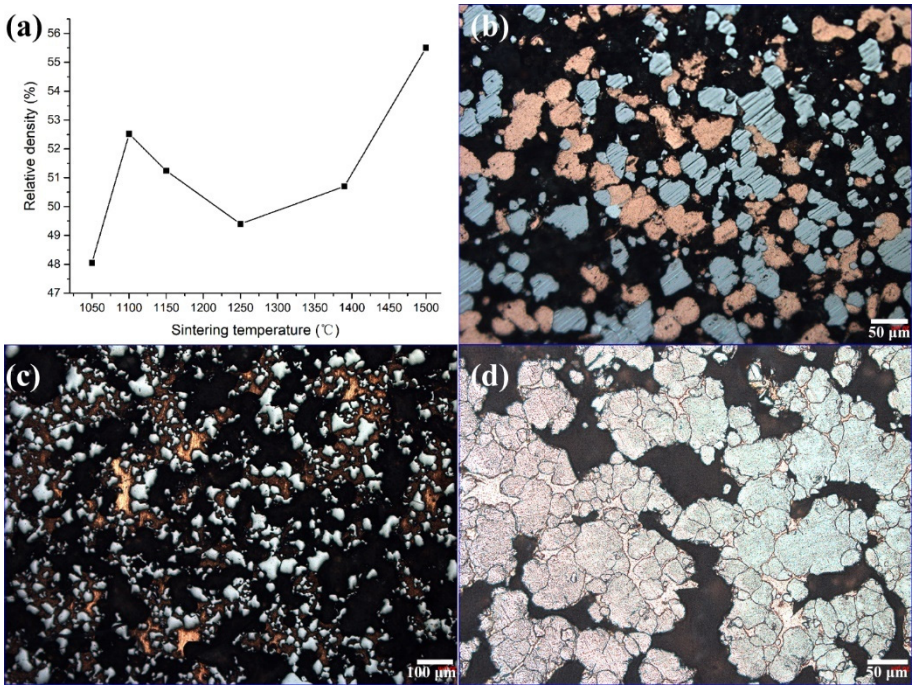


Figure 4. Microstructure of the MIM SCLs sintered at different temperatures. (**a**) Effects of sintering temperatures on the density of the samples. (**b**) 1050 °C. (**c**) 1100 °C. (**d**) 1500 °C.

3.2. Penetration Performance

The explosive test results are listed in Table 2. It is clear that the specimen sintered at 1100 °C shows a higher penetration depth than that sintered at 1050 °C. In addition, the MIM SCLs achieve comparable or even higher penetration depth than those prepared by spinning. Noticeably, the mass of the SCL produced by spinning is 70 g, which is much higher than approximately 59 g of those prepared by MIM with similar shape and size. In contrast, the SCL sintered at 1100 °C exhibits approximately 10% more depth than the spun SCL. The penetrated steel plate and concrete target are shown in Figure 5. It is obvious that the spun SCL has a small hole, which proves that the jet is almost coherent. By comparison, the hole formed by the MIM SCL is much bigger and radial curves around the hole are observed, which prove that the jet is noncoherent and radially spread out. The hole size is listed in Table 2 in which the sample sintered at 1050 °C shows higher noncoherence by forming bigger holes. Interestingly, Sun [11] reported that the penetration depth of CuSn10 SCL generated by machined and additively manufactured reaches about 168 mm and 214 mm, respectively. Similar results were also reported in [18]. These values are much lower than the present work, as shown in Table 2, which makes it quite reasonable that the MIM is an efficient way to fabricating SCLs.

It is well-known that the melting point and hardness of copper are much lower than those of steel. During penetration, the copper phase squeezed out suffers from melting, solidification, and formation of a Cu-rich layer in the steel. As a result, the tungsten particles play the most crucial role in determining the penetration performance in the concrete target. Thus, particle size is an important factor for consideration. The effects of the tungsten particle size on the density and penetration depth are listed in Table 2. The particle size shows negligible effect on the relative density because solid sintering of tungsten is rare at the temperature far below the melting point [19]. However, the penetration depth strongly depends on the particle size. The SCLs prepared using the −70-mesh powder shows inferior penetration ability than the sample prepared by spinning or that prepared using the original powder. As the particle size decreases, the penetration depth significantly increases. The sample prepared using the −250-mesh powder shows the best penetration ability, which is 18.44% higher than the sample prepared by spinning. The more refined powder using the −400-mesh impairs the penetration ability. The jet of the refined particles

is more noncoherent. Because of the sophisticated attack mechanism of a discontinuous jet on a target composed of two steel plates and concrete, the detailed mechanism of the tungsten particle size will be analyzed in a subsequent work. From the aforementioned tests, the best penetration depth can be obtained by choosing an appropriate tungsten particle size.

From the observation of the ballistic surface of the concrete target (Figure 5), no slug is found, which proves that almost all of the MIM SCL mass is used in forming a jet. Figure 6 shows that the SEM images and energy dispersive X-ray spectroscopy (EDS) results of the steel plate and concrete target. It is obvious that there exist numerous particles on the ballistic surface of steel and concrete target, as shown in Figure 6a,c. Additionally, the EDS results show that these particles contain a large fraction of W and a certain content of Cu. Further observation found that the content of Cu on the surface of concrete target is much lower than that on the steel surface, as shown in Figure 6b,d. Proving the existence of numerous tungsten particles, and a higher copper content is found at the surface of the steel plate than in the concrete. The particle size of them is a litter bit smaller (30–90 μm) than that of the particles before sintering. Most particles after test are slightly elongated, which proves that they have suffered from a considerable level of plastic deformation. However, the tungsten particles show no obvious characteristics of severe deformation, such as significantly elongated fragments (whisker shape). For the dense SCLs, the tungsten skeleton suffers from severe deformation and deforms into a continuous jet. The jet is broken into fragments during the penetration [16]. However, in the current MIM SCLs, the jet reflects the sum of the powder particles instead of a continuous structure.

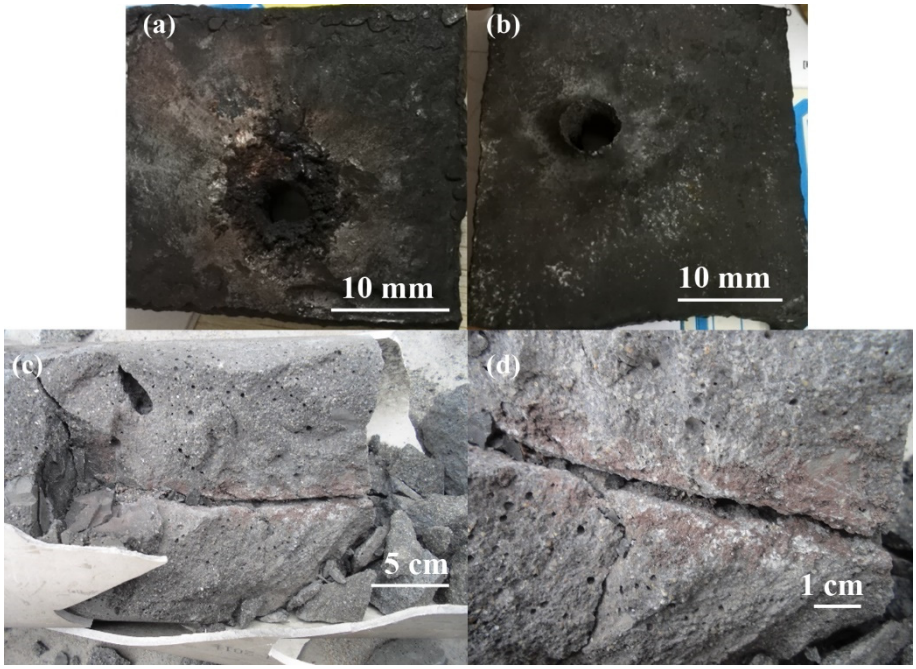


Figure 5. Steel plate and concrete target after the explosive test. (**a**) Steel plate penetrated by the MIM SCL. (**b**) Steel plate penetrated by the spun SCL. (**c**,**d**) Concrete target penetrated by the MIM SCL.

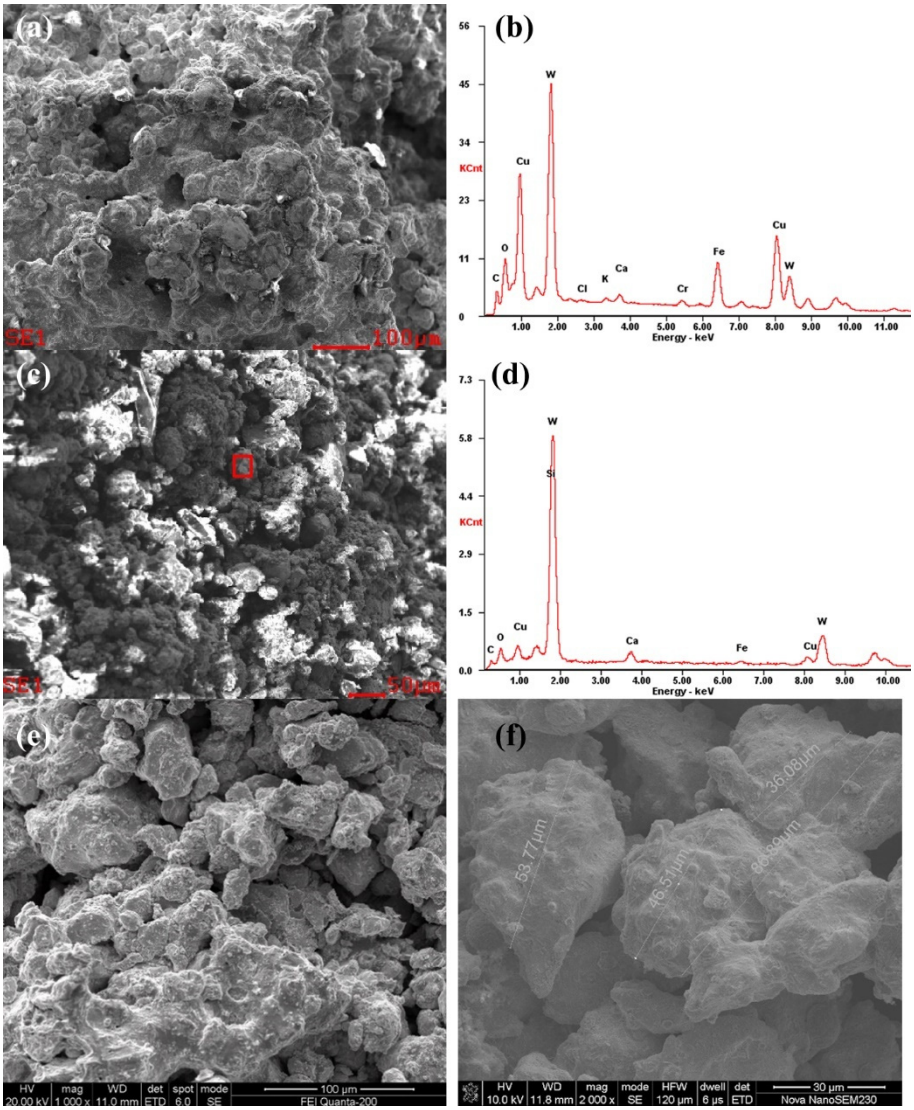


Figure 6. (**a**,**b**) SEM and EDS results of the ballistic surface of steel. (**c**,**d**) SEM and EDS results of the ballistic surface of the concrete target. (**e**,**f**) SEM images of the tungsten particles at the end of the ballistic channel.

3.3. Jet Characteristics

From the work of Li on porous SCL, slug is not likely to form at a porosity of 10–15%, which is much lower than the approximately 47–52% achieved in the present work [20]. Thus, formation of a slug by the MIM SCL is impossible. Under the condition of dense SCL, the tungsten skeleton breaks first. The deformation, fraction, and granulation of the skeleton largely use up the explosive energy of the SCL [21]. Meanwhile, copper undergoes large plastic deformation, recrystallization, and even melting. Liquid copper plays a role in lubricating the ballistics, which accelerates the penetration of the tungsten particles [22]. However, in a porous SCL composed of disconnected particles, destroying the W skeleton is not necessary. Instead, the SCL is rapidly compressed and densified [23]. In these processes, the jet temperature is increased under ultra-high pressure. The jet adiabatic temperature increases with the porosity. In the work of Li, 30% porosity led to a 1000 °C temperature increase [20]. As a result, the dynamic yield strength of the jet decreased, whereas the elongation increased, which increased the length of the jet, although it is a sum of discontinued particles, and hence improved the penetration ability. Thus, although the mass and relative density of the MIM SCLs were lower than those of the spun SCL, the penetration ability is comparable or even better. Meanwhile, seldom copper has been found

in the ballistic surface, which reflects that the lubrication effect of copper is not obvious. Sun's work found that large porosity led to shock-induced chemical reaction of the reactive powder material and hence reduce their penetration ability, but such a reaction was not found in current work prepared from more stable W-Cu system [24].

However, higher porosity decreases the coherence of the jet. The sonic criterion combines coherence with the volume sonic velocity of the SCL material [25]. The collapse velocity of SCL (V_0) is compared with its volume sonic velocity (c_0). When $V_0 \leq c_0$, the jet is coherent. When $V_0 > c_0$ and $\beta > \beta_c$, the jet is noncoherent, where β is the collapse angle and β_c is the maximum angle that an attached shock wave can form at a supersonic velocity. When $V_0 > c_0$ and $\beta < \beta_c$, no jet is formed (this condition is not considered because the jet has already been formed in this work). V_0 can be calculated by the following equation:

$$V_0 = \sqrt{2E_g} f(\mu) = \sqrt{2E_g}\left[\frac{C}{M} + \frac{n}{n+2}\right]^{\frac{1}{2}} \quad (1)$$

where C is the mass of the explosive charge, M is the mass of SCL, and n is the space geometric constant (0, 1, and 2 for the space, cylinder, and spherical shape, respectively). E_g is the Gurney energy of the explosive charge. From the calculation, V_0 is approximately 3.3 km/s (for M = 60 g). c_0 can be calculated by the following equation:

$$c_0 = \sqrt{\frac{K}{\rho}} \quad (2)$$

where K and ρ are the elastic modulus and density of the material, respectively. The calculated c_0 value is only 2.8 km/s (for the sample sintered using the original tungsten particle at 1100 °C). Thus, the jet is noncoherent, which aggravates the consumption of jet energy on the penetration direction and degrades the penetration effect. Because of the higher density, the samples sintered at 1100 °C exhibit higher coherence than those sintered at 1050 °C.

3.4. Effects of the SCL Mass

Because the relative density of the MIM SCL and the jet coherence can hardly be improved, increasing the mass of the SCL is an easier way to further improve the penetration depth. The mold is redesigned, and the height of the mouth part is improved. However, the larger volume of the SCL reduces the volume for explosive charge. Thus, the 70-g mass is the maximum mass under the current design condition. By increasing the height of the mouth part, the total height of the SCL can be increased by approximately 1–2 mm, and the mass can reach 65 or even 70 g. The results of the explosive tests are listed in Table 3. It is clear that the average penetration depth of the SCL with a 65-g mass reaches 745 mm. However, the distribution width is approximately 155 mm, which is smaller than that of the 59-g mass. The average penetration depth of the 70-g sample reaches 808 mm, and the penetration stability is better (60 mm). The noncoherence of the improved jet is slightly higher than that of the 59-g sample because improving the mass does not lead to the increase in the SCL density. Our subsequent work will try to improve the density of the SCL at a proper level to improve the mass and reduce the noncoherence of the jet.

Table 3. Effects of the SCL mass on the penetration performance.

Average Mass (g)	Height of SCL (mm)	Average Penetration Depth (mm)	Minimum Penetration Depth (mm)	Maximum Penetration Depth (mm)	Size of Ballistic Hole (mm)
59.23 (±0.54)	41.47 (±0.14)	650	560	730	8.5 × 8.2
65.68 (±0.68)	43.03 (±0.13)	745	650	805	9.0 × 8.3
69.72 (±1.65)	44.45 (±0.65)	808	780	840	9.1 × 8.5

4. Conclusions

The MIM method was applied to manufacture the W-Cu SCL, and the effects of density, tungsten particle size, and mass of the MIM W-Cu SCL on the penetration ability were studied for the first time. The main findings are concluded as follows:

1. The MIM W–Cu SCL, which is sintered at 1100 °C, can obtain a relative density of 52.52%, which is suitable for subsequent explosive tests. Higher sintering temperature leads to separation of W and Cu, cracks, and distortion, which is not conducive for its application.
2. The penetration ability of the MIM SCL exceeds that of the SCL produced by spinning. The −250-mesh tungsten powder reaches 700 mm, which is 18.44% higher than that of the SCL produced by spinning.
3. The penetration tests show that the MIM SCL has no slug and the jet consists of discontinuous tungsten particles. However, the jet is noncoherent.
4. Increasing the mass of the sample enhances the penetration depth. When the mass of the MIM SCL is almost equivalent to the spun SCL, the penetration depth exceeds 42.13% of the spun SCL.

Author Contributions: Conceptualization, H.H.; Data curation, Y.C. and X.Z.; Formal analysis, C.A.; Investigation, Z.H.; Methodology, Y.H.; Resources, Y.L. All authors have read and agreed to the published version of the manuscript.

Funding: This research was funded by the National Natural Science Foundation of China (Grant No. 52164042) and Guangxi Science and Technology Plan Project (Grant No. AD21220139).

Institutional Review Board Statement: Not applicable.

Informed Consent Statement: Not applicable.

Data Availability Statement: Data sharing is not applicable.

Acknowledgments: The use of facilities in State Key Laboratory for Powder Metallurgy at Central South University is acknowledged.

Conflicts of Interest: The authors declare no conflict of interest.

References

1. Li, G.; Chen, X.W. Selection and analysis of material models in copper jet penetration into water. *J. Phys. Conf. Ser.* **2020**, *1507*, 032017. [CrossRef]
2. Guo, W.; Liu, J.; Xiao, Y.; Li, S.; Zhao, Z.; Cao, J. Comparison of penetration performance and penetration mechanism of w-cu shaped charge liner against three kinds of target: Pure copper, carbon steel and Ti-6Al-4V alloy. *Int. J. Refract. Met. Hard Mater.* **2016**, *60*, 147–153. [CrossRef]
3. Lou, J.; Gabbitas, B.; Yang, F.; Raynova, S.; Lu, H. Effects of LaB6 additions on the microstructure and mechanical properties of a sintered and hot worked P/M Ti alloy. *J. Alloys Compd.* **2016**, *674*, 116–124. [CrossRef]
4. Zhou, C.; Yi, J.; Luo, S. Sintering High Tungsten Content W-Ni-Fe Heavy Alloys by Microwave Radiation. *Met. Mater. Trans. A* **2013**, *45*, 455–463. [CrossRef]
5. Guo, W.; Li, S.; Wang, F.; Wang, M. Dynamic recrystallization of tungsten in a shaped charge liner. *Scr. Mater.* **2009**, *60*, 329–332. [CrossRef]
6. Lawrie, J.J.; Mostert, F.J.; König, P.J.; Werneyer, K.D. The Use of the Gamma-Ray Absorption Technique as a Quality Control Procedure in the Manufacture of Powder Metal Shaped Charge Liners. *J. Appl. Mech.* **2010**, *77*, 1701. [CrossRef]
7. Yan, Z.; Xu, G.; Suo, J. Study on W/(TiN)Ta composite and its application in shape charge liner. *SN Appl. Sci.* **2020**, *10*, 1736. [CrossRef]
8. Lu, C.; Liu, J.; Li, S. Penetration Performance of W-Ni-Fe Alloy Shaped Charge Line. *Rare Met. Mater. Eng.* **2013**, *42*, 2337–2340.
9. Xi, B.; Liu, J.; Li, S.; Lv, C.; Guo, W.; Wu, T. Effect of interaction mechanism between jet and target on penetration performance of shaped charge liner. *Mater. Sci. Eng. A* **2012**, *553*, 142–148. [CrossRef]
10. Lou, J.; Gabbitas, B.; Zhang, D. Improving the uniformity in mechanical properties of a sintered Ti compact using a trace amount of internal lubricant. *J. Mater. Process. Technol.* **2014**, *214*, 1798–1805. [CrossRef]
11. Sun, S.; Jiang, J.; Wang, S.; Men, J.; Li, M.; Wang, Y. Comparison of Shaped Charge Jet Performance Generated by Machined and Additively Manufactured CuSn10 Liners. *Materials* **2021**, *14*, 7149. [CrossRef] [PubMed]

12. Lou, J.; Li, Y.; He, H.; Li, D.; Wang, G.; Feng, J.; Liu, C. Interface development and numerical simulation of powder co-injection moulding. Part. I. Experimental results on the flow behaviour and die filling process. *Powder Technol.* **2017**, *305*, 405–410. [CrossRef]
13. He, H.; Li, Y.; Lou, J.; Li, D.; Liu, C. Prediction of density variation in powder injection moulding-filling process by using granular modelling with interstitial power-law fluid. *Powder Technol.* **2015**, *291*, 52–59. [CrossRef]
14. Mahdian, A.; Liaghat, G.H.; Ghayour, M. Generalized closed-form model for analysis of asymmetric shaped charges. *J. Appl. Mech. Tech. Phys.* **2013**, *54*, 259–267. [CrossRef]
15. Zhang, Z.; Wang, L.; Silberschmidt, V.V. Damage response of steel plate to underwater explosion: Effect of shaped charge liner. *Int. J. Impact Eng.* **2017**, *103*, 38–49. [CrossRef]
16. Molinari, J. Finite element simulation of shaped charges. *Finite Elem. Anal. Des.* **2002**, *38*, 921–936. [CrossRef]
17. Alvarado-Contreras, J.A.; German, R.M.; Maximenko, A.L.; Olevsky, E.A. Coupled Densification—Shape Distortion Analysis of Liquid Phase Sintering Affected by Gravity. *Met. Mater. Trans. A* **2013**, *45*, 927–933. [CrossRef]
18. Guo, X.; Huang, S.; Song, P.; Li, Y.; Liu, J.; Guo, M. Additive manufacturing of copper alloy and its application in Munroe effects. In *AOPC 2020: Advanced Laser Technology and Application*; International Society for Optics and Photonics: Bellingham, WA, USA, 2020; p. 11562.
19. Zou, J.; Song, D.; Shi, H.; Liang, S. Effects of grading tungsten powders on properties of CuW alloy. *Mater. Res. Express* **2020**, *7*, 026528. [CrossRef]
20. Li, R. *Study on the Jet Mechanisms of Shaped Charge with Porous Liner and its Applications*; University of Science and Technology of China: Hefei, China, 2008.
21. Perez-Soriano, E.M.; Arévalo, C.; Montealegre-Meléndez, I.; Neubauer, E.; Kitzmantel, M. Influence of starting powders on the final properties of W-Cu alloys manufactured through rapid sinter pressing technique. *Powder Met.* **2020**, *64*, 75–81. [CrossRef]
22. Zhao, Z.; Liu, J.; Guo, W.; Li, S.; Wang, G. Effect of Zn and Ni added in W–Cu alloy on penetration performance and penetration mechanism of shaped charge liner. *Int. J. Refract. Met. Hard Mater.* **2016**, *54*, 90–97. [CrossRef]
23. Cui, P.; Shi, D.; Xu, J.; Wang, T.; Zhang, X.; Li, Z.; Wang, D. Numerical Simulation on Jet Forming and Penetration Performance of Several Amorphous Energetic Alloy Liner with Typical Structures. *J. Phys. Conf. Ser.* **2021**, *1948*, 012186. [CrossRef]
24. Sun, M.; Li, C.; Zhang, X.; Hu, X.; Hu, X.; Liu, Y. Reactivity and Penetration Performance Ni-Al and Cu-Ni-Al Mixtures as Shaped Charge Liner Materials. *Materials* **2018**, *11*, 2267. [CrossRef] [PubMed]
25. Elshenawy, T.; Elbeih, A.; Li, Q. Influence of target strength on the penetration depth of shaped charge jets into RHA targets. *Int. J. Mech. Sci.* **2018**, *136*, 234–242. [CrossRef]